Cover Sheet

Statement: This manuscript is a non-peer reviewed preprint submitted to EarthArXiv.

Journal submission: Not applicable.

Authors and ORCID:

O.L. Konovalov — Head of Laboratory, ITKG, Belarusian State University, PhD (Engineering), Associate Professor.
Email: konovalov@bsu.by
ORCID: https://orcid.org/0009-0009-6367-4655

V.V. Krasnoproshin — Professor, Department of ISU, Belarusian State University, D.Sc. (Engineering).
Email: krasnoproshin@bsu.by

Title: Three-Dimensional Modeling of the Underground Mineral Extraction Process: A Dynamic Three-Dimensional Model of Underground Mining Space

Keywords: digital twin, underground mining, 3D modeling, sweep surface, loft surface, contour fitting, gradient descent, laser scanning, computational geometry, bedded deposits.

Three-Dimensional Modeling of the Underground Mineral Extraction Process: A Dynamic Three-Dimensional Model of Underground Mining Space

O.L. Konovalov* V.V. Krasnoproshin†

Abstract

Three-dimensional models of underground space are a core component of digital twins of mining enterprises. The fundamental requirement for such models is that they must be dynamic — accurately reflecting the current state of their physical counterpart at each moment in time. When developing large underground bedded mineral deposits (coal, potash), the mined horizon constitutes a continuously changing network of hundreds of openings with complex topology. Existing approaches based on sweep bodies with Boolean operations are critically resource-intensive for such scale, while loft representations based on vertical cross-sections suffer from shape distortion. This paper proposes a hybrid geometric representation that combines the accuracy of the sweep approach with the non-intersection property of the loft approach. The key idea is to decompose each excavation into a set of loft bodies corresponding to individual passes of the mining machine. An efficient analytical algorithm is developed for constructing vertical cross-sections of normal profile bodies (NP-bodies) without explicit 3D surface computation, exploiting the property that the projection of a helical sweep surface onto the horizontal plane is a circle for each fixed profile parameter. An inverse contour fitting algorithm based on gradient descent is proposed for recovering NP-body trajectory parameters from scanned cross-section data. Experimental validation using underground laser scanning data from a potash deposit demonstrates contour recovery accuracy of 0.05 m and surface deviation of 0.07 m, with gradient descent convergence in 14–32 iterations. The approach is suitable for most digital twin tasks including equipment placement, ventilation calculation, and transport route planning.

Keywords: digital twin, underground mining, 3D modeling, sweep surface, loft surface, contour fitting, gradient descent, laser scanning, computational geometry, bedded deposits.

*Head of Laboratory, ITKG, Belarusian State University, PhD (Engineering), Associate Professor. Email: `konovalov@bsu.by`. ORCID: https://orcid.org/0009-0009-6367-4655

†Professor, Department of ISU, Belarusian State University, D.Sc. (Engineering). Email: `krasnoproshin@bsu.by`

1 Introduction

Digital twins of mining enterprises represent a new paradigm in mine management, enabling real-time monitoring of production processes, predictive maintenance of equipment, simulation of ventilation networks, and proactive assessment of safety risks [1, 12]. The relevance of digital twin technology is driven by the increasing complexity of underground mining operations, the need to reduce operational costs while maintaining safety standards, and the growing adoption of Industry 4.0 technologies in the mining sector.

Three-dimensional models of underground space form the foundation of digital twins of mining enterprises [1]. The fundamental requirement for a 3D model of a digital twin is that it must be "dynamic" — at each moment in time (within a specified time interval), it must represent an accurate reflection of the current state of its physical counterpart [1, 9].

Three-dimensional virtual models constitute the core of a digital twin, as they reproduce the behavior, characteristics, and dynamics of a physical object in a computational environment. They represent a computational representation of a physical entity. These models are updated with real-time data to reflect the state and behavior of the physical counterpart [1].

In the development of large underground bedded mineral deposits (coal and potash deposits), the underground space of the mined horizon typically constitutes a continuously changing network consisting of hundreds of openings and intersection chambers with complex topology. In two-dimensional geological and mine surveying models, the required "dynamicity" was achieved quite some time ago. An example is the automated geological and mine surveying support system of OAO "Belaruskali" [2], in which the mine plan is updated within a few hours after the mine surveyor has completed the latest measurement.

When transitioning to three-dimensional models, the situation becomes significantly more complex. This is due to the fact that a 3D model is considerably more resource-intensive in terms of its construction, storage, and visualization. The use of standard CAD tools for creating and updating such a model is not feasible, as it requires a large volume of manual operations and additional technological information that does not currently exist (the precise spatial trajectory of the extraction machine).

Practical implementation of a 3D model requires that its construction technology be maximally adapted to existing mine surveying methods and require minimal additional effort from specialists.

Furthermore, it appears evident that the use of CAD representations is, to a certain extent, "redundant" for describing 3D underground openings, where centimeter-level accuracy is generally sufficient. For practical implementation of 3D models, a "simplified" representation is needed that, on the one hand, describes the 3D geometry of underground mining objects with specified accuracy, and, on the other hand, in terms of model resource intensity (storage, construction, rendering), approaches that of 2D analogs.

Several approaches to 3D modeling of underground excavations have been proposed in recent years. Yang et al. [10] developed a parametric tunnel modeling method using CAD and Unity3D with curve lofting algorithms for handling inflection points and intersections. Zhang et al. [11] proposed a point cloud-based method for coal mine tunnel modeling using Poisson surface reconstruction, achieving high geometric fidelity. Cui et al. [12] introduced a multiscale digital twin framework integrating global tunnel network topology with local point cloud reconstruction. However, these methods either rely on high-density scanning data, are designed for specific mining conditions, or do not address the challenge of dynamic model updating in real mining operations involving hundreds of intersecting openings.

2 Analysis of the Problem and Problem Formulation

The most natural geometric representation of a 3D model of an underground opening is a sweep body [3], where the standard cutting profile of the mining machine serves as the contour, and the 3D trajectory of the machine during excavation serves as the guide curve (Fig. 1a).

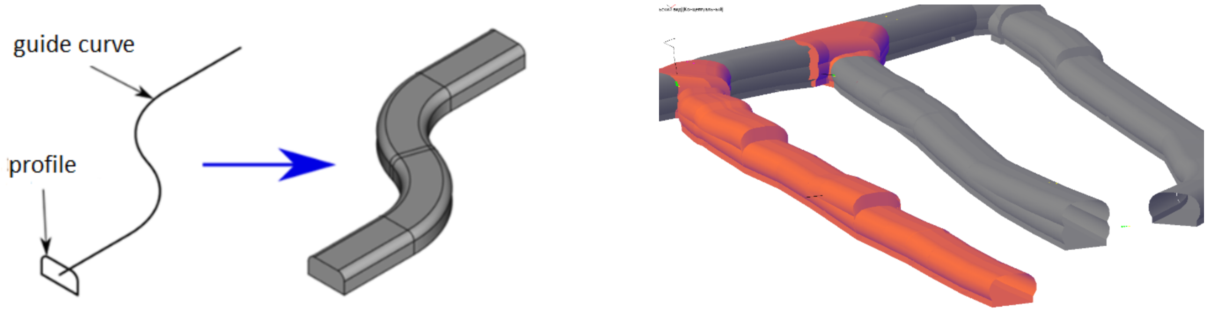

(a) Sweep body (b) Multiple passes

Figure 1: Geometric representation of an underground opening.

However, a real underground opening, at significant dip angles of the enclosing horizons, is formed as a result of several passes of the mining machine (Fig. 1b). To obtain a 3D model of such an opening, a series of Boolean union operations must be performed over an intersecting set of sweep bodies. Such a model would reproduce the shape of the opening with maximum accuracy; however, the sequential union of multiple 3D bodies leads to a sharp increase in the number of small facets at the intersection regions. Even though each new pass intersects only with its nearest neighboring segments, the computer would expend too many resources computing surfaces at the intersection zones [4]. Due to the high computational load and inevitable rounding errors, this method becomes inefficient for modeling large-scale mining objects. An underground horizon may contain hundreds of intersecting passes, making the process of constructing a 3D model based on sweep bodies critically resource-intensive. Moreover, constructing such a model requires precise information about the machine trajectory during each pass, which is generally unknown.

An alternative approach to constructing a 3D model is based on the concept of an "excavation" — the excavated space (3D body) corresponding to the volume of mining space between two vertical cross-sections [5]. In this case, the surface of the excavation is represented as a loft surface [3] constructed between these sections (Fig. 2a).

The principal advantage of this representation of a 3D model of underground space is that the bodies constructed for adjacent vertical cross-sections do not intersect. This property significantly simplifies operations with the model, in particular: volume calculation, model updating, equipment placement, and construction and analysis of networks (transport, power, ventilation, etc.).

Despite this advantage, the loft representation based on vertical cross-sections has not yet been widely adopted for creating dynamic 3D models. This is due to the fact that constructing a loft surface from two end sections can significantly distort the shape of

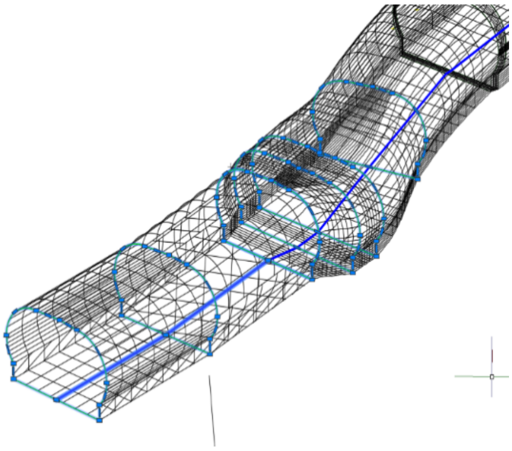

(a) Loft surfaces between sections

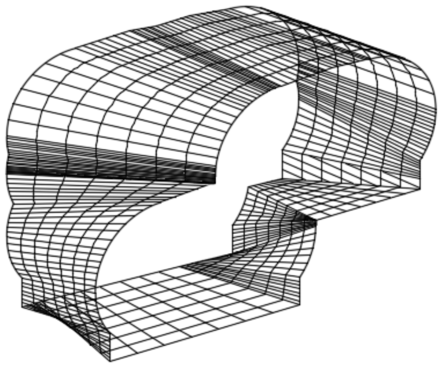

(b) Form distortion

Figure 2: Loft representation of an excavation.

the opening. This is particularly evident when the parameterizations of the end sections differ substantially (Fig. 2b).

We propose a new, specialized geometric representation of a mining opening that combines the advantages of both approaches: the accuracy of the sweep representation and the non-intersection property of the loft representation. Remaining within the loft paradigm (where the input information for construction consists of the end vertical cross-sections), we propose to decompose the excavation body into a set of loft bodies, each corresponding to an individual pass of the mining machine that forms the excavation. To achieve this, both end vertical cross-sections must be decomposed into pairs of vertical cross-sections for each pass, and a separate loft body is constructed for each pair. The excavation itself is then obtained as the union of the constructed loft bodies.

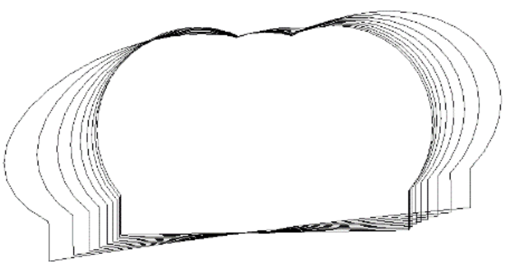

(a) Vertical cross-sections generation

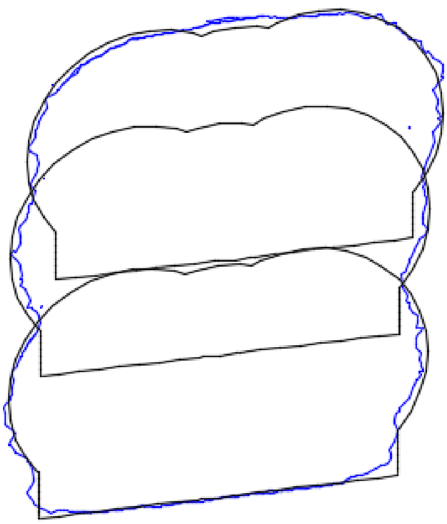

(b) Contour fitting result

Figure 3: Proposed approach: cross-section generation and contour fitting.

The fundamental element of the proposed approach is an algorithm for generating the vertical cross-section of a single pass, taking into account its inclination and turning radius, as well as its orientation relative to the section plane (Fig. 3a). Based on this algorithm, a specialized contour fitting algorithm [6] is proposed, which performs the fitting of a set of vertical cross-sections — constructed by the base algorithm — to the actual scanned vertical cross-section. As a result, a set of profiles is obtained that approximates the real contour of the opening with maximum accuracy (Fig. 3b).

The described approach allows us to formulate the general objective of this study: to develop a 3D model of underground mining operations, as well as a technology for its construction, ensuring high geometric accuracy at minimal labor cost.

3 Parametric Profile of the Mining Machine, Concepts of NP-Body and NP-Excavation

The fundamental geometric figure that shapes the geometry of underground space is the standard cutting profile of the mining machine during horizontal rectilinear motion in an undisturbed rock mass. Such a profile can be represented as a planar figure F obtained by the union of a set of simple convex figures (circle, rectangle, triangle), the dimensions and relative positions of which are determined by a set of technological parameters of the mining machine. A typical cutting profile of a mining machine is shown in Fig. 4. In this case, the set of technological parameters describing the standard profile can be represented as a vector $\mathbf{p} = (R, D, H, d, h)$. The profile corresponding to a specific set of parameters will be denoted $F(\mathbf{p})$. The profile is the union of parameterized simple convex figures whose positions are defined in the local coordinate system of the profile:

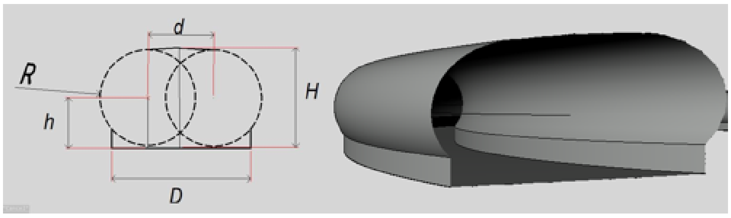

Figure 4: Typical cutting profile of a mining machine.

$$F(\mathbf{p}) = \bigcup_{i=1}^{K} f_i(\mathbf{p}) \tag{1}$$

The surface of a single pass is the locus of points of the contour of a specific profile $F(\mathbf{p})$ as it moves along a spatial curve coinciding with the trajectory of the mining machine. This type of surface representation is widely used in modern CAD systems and belongs to the class of sweep surfaces [1]. In the general case, sweep surfaces are two-parametric and are obtained by moving a one-parametric planar contour $C(u)$ along a spatial guide curve $T(s)$.

For the surface of a single opening, the planar contour $C(u)$ is the contour of the standard cutting profile of the machine $\partial F(\mathbf{p})$, parameterized along its length. The guide curve $T(s)$ is the trajectory of the machine (Fig. 1).

The boundary positions of the profile $F_0(\mathbf{p})$, $F_1(\mathbf{p})$ corresponding to the extreme values s_0, s_1 will be called the *end faces* of the sweep surface. The volume bounded by the sweep surface and its end faces will be called the *sweep body*.

The mine design methodology and the technological constraints on the motion of the mining machine are such that, when modeling the surface of a single pass, it is sufficient to consider three types of spatial segments as guide curves: a linear segment, a circular arc, and a helical segment (helix).

All three types of segments can be described by a common set of parameters. A helical segment can be defined by its length l, radius R, and pitch h. A linear segment and a circular arc can be considered as special cases of the helical segment, where $R \to \infty$ and $h = 0$, respectively. The technological constraints of each mining machine imply certain restrictions on the limiting values of these parameters. For example, these include the minimum turning radius $r_{\min}$ ($r > r_{\min}$) and the maximum helix pitch $h_{\max}$ ($h < h_{\max}$).

A guide curve whose segments satisfy the specified constraints will be called a *canonical trajectory*.

The set of parameters describing a canonical segment of the guide curve D can be represented as a vector $\mathbf{d} = (l, r, h)$.

Then, the 3D sweep body formed by the contour of the standard cutting profile $F(\mathbf{p})$, where the guide curve is a segment of the canonical trajectory $D(\mathbf{d})$, will be called a *normal profile body* (NP-body) and denoted $\mathrm{NP}(\mathbf{p}, \mathbf{d})$.

Let us define the concept of a vertical cross-section of an NP-body by a plane P. Assume that D intersects P and the end faces lie on opposite sides of the plane P. Then, the set of points of the plane P belonging to the NP-body will be called the *vertical cross-section* and denoted $\mathrm{VC}(\mathbf{p}, \mathbf{d}, P)$. By definition, the vertical cross-section is a planar spatial figure.

3.1 Concept of NP-Excavation and Loft-Excavation

The fundamental primitive of the proposed 3D model of underground space is the *excavation U* — the excavated space (3D body) corresponding to the volume of mining space between two boundary vertical cross-sections V_0 and V_1. A vertical cross-section V is a planar spatial figure lying in the vertical section plane P, defined by a point on the plane P_0 and a normal P_n.

Assume that a set of NP-bodies $G = \{\mathrm{NP}_j\}_{j=1}^{k}$ of all passes forming the volume of excavated space between two vertical cross-sections V_0 and V_1 is given. The NP-excavation U will be a 3D body obtained as a result of the Boolean union of all bodies from G, followed by subtraction of two boundary half-spaces H_0 and H_1 defined by the planes of the vertical cross-sections P_0 and P_1. Here, the half-spaces H_0 and H_1 are assumed to be positioned such that the volume of the excavation belongs to their intersection $H_0 \cap H_1$, while the end faces of all bodies from G do not belong to it:

$$U_{np} = \left\{ \mathbf{x} \in \mathbb{R}^3 \, : \, \mathbf{x} \in \bigcup_{j=1}^{k} \mathrm{NP}_j, \quad \mathbf{x} \in H_0 \cap H_1 \right\} \tag{2}$$

The NP-excavation accurately describes the opening; however, its construction requires precise information about the trajectories of each NP-body. Therefore, we proceed to the description of the loft representation of the excavation.

The set G uniquely induces a decomposition of each boundary section V^m into a union of vertical cross-sections of NP-bodies:

$$V^m = \bigcup_{j=1}^{k} \mathrm{VC}(\mathbf{p}_j, \mathbf{d}_j, P^m) \tag{3}$$

For each pair of vertical cross-sections $\mathrm{VC}(\mathbf{p}_j, \mathbf{d}_j, P^0)$ and $\mathrm{VC}(\mathbf{p}_j, \mathbf{d}_j, P^1)$, a corresponding loft body $\mathrm{LB}(\mathbf{p}_j, \mathbf{d}_j)$ is constructed. The *loft-excavation* is defined as the union of all such bodies:

$$U_{lf} = \bigcup_{j=1}^{k} \mathrm{LB}(\mathbf{p}_j, \mathbf{d}_j) \tag{4}$$

The principal advantage of the loft representation is that it can be constructed without knowledge of the guide curve parameters. It is sufficient to know the decomposition of the boundary cross-sections.

4 Vertical Cross-Section of an NP-Body: An Efficient Algorithm

Consider an efficient algorithm for constructing the vertical cross-section of an NP-body, where efficiency implies that the 3D representation of the body is not explicitly constructed, and no direct intersection with the plane is performed.

To obtain the vertical cross-section $\mathrm{VC}(\mathbf{p}, \mathbf{d}, P)$ of an NP-body, one can construct sweep surfaces for all simple figures of the standard profile $F = \{f(\mathbf{p}_i)\}_{i=1}^{K}$ (Fig. 5a), construct the vertical cross-section of each such surface with the plane P, and then perform the union of the resulting closed contours (Fig. 5b). A similar approach is used in [7].

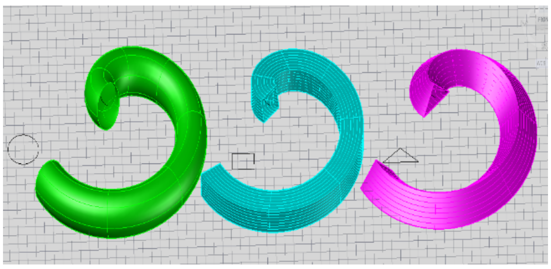

(a) Sweep surfaces for simple figures

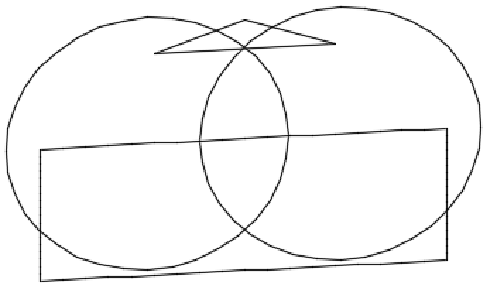

(b) Union of closed contours

Figure 5: Construction of the vertical cross-section of an NP-body.

For this purpose, it is sufficient to consider the construction of cross-sections for helical surfaces generated by three types of curves: a circle, a horizontal segment, and a vertical segment. In the general case, this is a challenging problem, since the equation describing the closed curve obtained in the plane of the vertical cross-section is transcendental in both surface parameters [8]. We show that such an equation can be solved explicitly when one of the parameters is fixed.

4.1 Helical Surface Generated by a Circle

The parametric equation of a helix with radius R and pitch h can be written as:

$$\vec{r}(t) = (R\cos t,\ R\sin t,\ ht) \tag{5}$$

The tangent vector is obtained by differentiation:

$$\vec{t} = \frac{d\vec{r}(t)}{dt} = (-R\sin t,\ R\cos t,\ h) \tag{6}$$

The normal vector is constructed as the normalized derivative of the tangent vector:

$$\vec{n}(t) = \frac{d\vec{t}/dt}{\|d\vec{t}/dt\|} = (-\cos t,\ -\sin t,\ 0) \tag{7}$$

The binormal vector is obtained as the cross product of the tangent and normal vectors:

$$\vec{b}(t) = \frac{1}{\|\vec{t}\|}\,\vec{t}\times\vec{n} = \frac{1}{\sqrt{R^2+h^2}}\,(h\sin t,\ -h\cos t,\ R) \tag{8}$$

Then, the parametric surface S swept by a circle of radius a, constructed in the plane defined by vectors $\vec{n}$ and $\vec{b}$, can be written as:

$$S(t,u) = \vec{r}(t) + a\,\vec{n}(t)\cos u + a\,\vec{b}(t)\sin u \tag{9}$$

where t is the parameter of the guide curve and u is the parameter of the swept contour, $u \in [0, 2\pi]$.

Writing the surface in coordinate form:

$$\begin{aligned} x(t,u) &= R\cos t - a\cos t\cos u + \frac{ha\sin t\sin u}{\sqrt{R^2+h^2}} \\ y(t,u) &= R\sin t - a\sin t\cos u - \frac{ha\cos t\sin u}{\sqrt{R^2+h^2}} \\ z(t,u) &= ht + \frac{Ra\sin u}{\sqrt{R^2+h^2}} \end{aligned} \tag{10}$$

The efficient algorithm for constructing the vertical cross-section is based on the following observation: the element of the surface S corresponding to a fixed value of the parameter u represents a segment of a helix, and its projection onto the horizontal plane represents a segment of a circle. This can be proved formally by writing $x^2(t,u)+y^2(t,u)$ using (10):

$$x^2(t,u)+y^2(t,u) = (R-a\cos u)^2 + \frac{h^2a^2\sin^2 u}{R^2+h^2} \tag{11}$$

Since the right-hand side does not contain the parameter t, for each fixed $u = u^*$, the points of the surface $S(t,u^*)$ form a circle of radius:

$$\rho(u^*) = \sqrt{(R-a\cos u^*)^2 + h^2a^2\sin^2 u^*/(R^2+h^2)}.$$

To approximately construct the cross-section, we first construct a set of planar concentric circles corresponding to a discrete set of parameters $u = \{u_1, u_2, \ldots, u_n\}$. We find the intersection of the circle corresponding to u^* with the line that is the projection of the vertical section plane P onto the horizontal plane. Let this be the point with coordinates $(x = A,\ y = B)$.

To find the coordinate Z, we express $\cos t$ through $\sin t$ using the first equation of (10):

$$\cos t = \frac{1}{R - a\cos u}\left(A - \sin t \cdot \frac{ha\sin u}{\sqrt{R^2 + h^2}}\right) \tag{12}$$

Substituting B and the obtained expression for $\cos t$ into the second equation of (10) and rearranging:

$$\sin t = \frac{S_{\text{up}}}{S_{\text{dw}}} \tag{13}$$

where

$$\begin{aligned} S_{\text{up}} &= B\,(R^2 + h^2)(R - a\cos u) + A\,ha\sin u\,\sqrt{R^2 + h^2} \\ S_{\text{dw}} &= (R - a\cos u)^2(R^2 + h^2) + (ha\sin u)^2 \end{aligned} \tag{14}$$

The ratio $S_{\text{up}}/S_{\text{dw}}$ must satisfy $|S_{\text{up}}/S_{\text{dw}}| \leq 1$ for a real solution to exist. Points where the condition is violated correspond to regions outside the surface and are excluded from the cross-section contour.

Using the arcsin function, we obtain $t^* = \arcsin(S_{\text{up}}/S_{\text{dw}})$. It should be noted that the arcsin function returns values in $[-\pi/2, \pi/2]$. Since the parameter t of the helix may take values outside this interval (particularly for long passes where $l > \pi R$), the correct branch is selected based on the sign of $\cos t$ computed from Eq. (12).

Then, using the third equation of (10):

$$Z = h\,t^* + \frac{Ra\sin u^*}{\sqrt{R^2 + h^2}} \tag{15}$$

The obtained analytical expression allows us to approximate the vertical cross-section as a polyline with any specified accuracy. No explicit 3D helical surface construction takes place. The computational complexity is linear in the number of approximation points.

Fig. 6a presents approximations of the profiles of vertical cross-sections parallel to the ZX plane, constructed with an angular step of 1.5°, for a helical cylindrical surface with parameters $R = 10$, $h = 2$, $a = 1.56$.

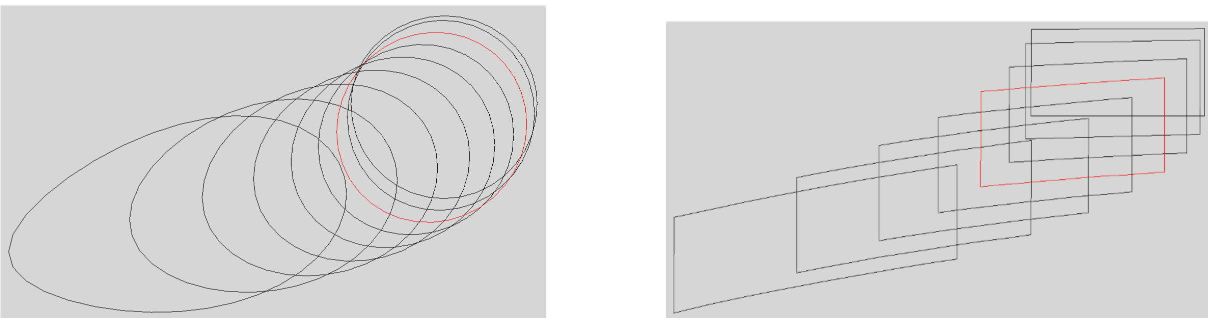

(a) Helical cylinder ($R = 10$, $h = 2$, $a = 1.56$)

(b) Helical box section ($R = 10$, $h = 2$, $c = 1$, $b = 2$)

Figure 6: Approximations of vertical cross-section profiles with 1.5° angular step.

4.2 Helical Surface Generated by a Horizontal Segment

The parametric surface S swept by a horizontal segment of length b located at a distance c from the guide curve:

$$S(t,u) = \vec{r}(t) + \vec{n}(t)\,(b - bu) + c\,\vec{b}(t) \tag{16}$$

where $u \in [0,1]$. Performing transformations analogous to the circle case, we obtain (13) with:

$$\begin{aligned} S_{\text{up}} &= B\,(R^2+h^2)(R-b(1-u)) + A\,hc\sqrt{R^2+h^2} \\ S_{\text{dw}} &= (R-b(1-u))^2(R^2+h^2) + (hc)^2 \end{aligned} \tag{17}$$

and $Z = h\,t^* + Rc/\sqrt{R^2+h^2}$.

4.3 Helical Surface Generated by a Vertical Segment

The parametric surface S swept by a vertical segment of length c located at a distance b from the guide curve:

$$S(t,u) = \vec{r}(t) + b\,\vec{n}(t) + cu\,\vec{b}(t) \tag{18}$$

Performing analogous transformations, we obtain (13) with:

$$\begin{aligned} S_{\text{up}} &= B\,(R-b) + \frac{A\,hcu}{\sqrt{R^2+h^2}} \\ S_{\text{dw}} &= (R-b)^2 + \frac{(hcu)^2}{R^2+h^2} \end{aligned} \tag{19}$$

Fig. 6b presents approximations for a helical box section with parameters $R = 10$, $h = 2$, $c = 1$, $b = 2$.

4.4 Degenerate Cases

The obtained formulas are valid for the general helical case ($R < \infty$, $h > 0$). For a circular arc ($h = 0$), the expressions simplify since $R^2 + h^2 = R^2$. For a linear segment ($R \to \infty$), the guide curve degenerates to a straight line, and the vertical cross-section is constructed directly as the translation of the profile contour — no helical surface computation is required.

4.5 Contour Union and Complexity

After the vertical cross-sections of the sweep surfaces of the simple figures have been obtained, the union of the resulting closed contours is performed. This can be done using a CAD kernel or external libraries such as CGAL (Computational Geometry Algorithms Library). The complexity of the union stage is $O(K \log K)$, where K is the number of approximation points. Since the complexity of constructing the individual cross-sections also does not exceed $O(K \log K)$, the algorithm is efficient as a whole.

5 Inverse Problem: Contour Fitting Algorithm

The algorithm in Section 4 constructs the vertical cross-section of an NP-body from given trajectory parameters and a section plane. This allows us to pose the inverse problem: given a digitized contour of a real opening, recover the parameters of the vertical cross-sections of the constituent NP-bodies. This problem belongs to the class of contour fitting problems [6].

Due to the complexity and non-smoothness of the approximation contour, classical methods (Fitzgibbons, Taubin) are not applicable. A modern approach based on gradient descent in the parameter space [6] is employed.

5.1 Input Data and Parameter Vector

Let the vertical section plane P be defined by a point $O \in \mathbb{R}^3$ and a unit normal $\vec{n}$. Introduce an orthonormal basis $\vec{e}_1, \vec{e}_2 \perp \vec{n}$ in the plane and the transition matrix $E = [\vec{e}_1 \;\; \vec{e}_2] \in \mathbb{R}^{3\times 2}$. Any point of P is written as $\mathbf{x} = O + E(\xi_1, \xi_2)^T$.

Let the scan point set be $D = \{\boldsymbol{\xi}_j\}_{j=1}^{N} \subset \mathbb{R}^2$. Define the sought parameter vector:

$$\boldsymbol{\vartheta} = \begin{pmatrix} \theta \\ h \\ \omega \\ \Delta\xi_1 \\ \Delta\xi_2 \end{pmatrix}, \tag{20}$$

where θ is the angle between the section plane and the trajectory tangent (rad); h is the helix pitch (m); ω is the radius of curvature (m); $\Delta\xi_1, \Delta\xi_2$ are displacement components (m).

5.2 Error Function

The vertical cross-section in local coordinates is defined by $s_0(u;\theta)$, $u \in [0,1]$. In global coordinates:

$$s(u;\boldsymbol{\vartheta}) = O + E[s_0(u;\theta) + \mathbf{t}], \quad \mathbf{t} = (\Delta\xi_1, \Delta\xi_2)^T. \tag{21}$$

The error function (sum of squared distances):

$$E(\boldsymbol{\vartheta}) = \sum_{j=1}^{N} \left\| \boldsymbol{\xi}_j - \left[s_0(u_j^*;\, \theta) + \mathbf{t} \right] \right\|^2, \tag{22}$$

where u_j^* is the parameter of the nearest point on s_0 to $\boldsymbol{\xi}_j - \mathbf{t}$.

5.3 Multiple NP-Bodies

For M NP-bodies, the scan point set D is shared — the bodies compete for points. The error function:

$$E(\{\boldsymbol{\vartheta}^{(m)}\}) = \sum_{j=1}^{N} \min_m \left\| \boldsymbol{\xi}_j - \left[s_0\!\left(u_j^*(\boldsymbol{\vartheta}^{(m)});\, \theta^{(m)} \right) + \mathbf{t}^{(m)} \right] \right\|^2. \tag{23}$$

Introducing the dynamic assignment

$$D^{(m)} = \left\{ \boldsymbol{\xi}_j \in D \,:\, m = \arg\min_k \left\| \boldsymbol{\xi}_j - \left[s_0\left(u_j^*(\boldsymbol{\vartheta}^{(k)});\, \theta^{(k)} \right) + \mathbf{t}^{(k)} \right] \right\| \right\}, \tag{24}$$

the error becomes $E = \sum_{m=1}^{M} \sum_{j \in D^{(m)}} \|\boldsymbol{\xi}_j - [s_0(u_j^*; \theta^{(m)}) + \mathbf{t}^{(m)}]\|^2$. The assignment is recomputed at each error evaluation, making E piecewise smooth. In practice, the fraction of switching points is negligible, and the finite-difference gradient remains well-behaved.

5.4 Gradient and Algorithm

The gradient is computed via central differences: $\partial E / \partial \vartheta_i \approx [E(\boldsymbol{\vartheta} + h_i \mathbf{e}_i) - E(\boldsymbol{\vartheta} - h_i \mathbf{e}_i)]/(2h_i)$, with $h_i = \varepsilon_{\text{rel}} \cdot |\vartheta_i|$ ($\varepsilon_{\text{rel}} = 10^{-4}$). The nearest-point search uses a k-d tree over the discretized cross-section ($K = 150$–250 points).

Table 1: Perturbation steps for finite-difference gradient.

Parameter	Typical range	Example h_i
θ (rad)	$0 - 10^{-1}$	$10^{-6} - 10^{-5}$
h (m)	$0 - 5$	$10^{-4} - 10^{-3}$
ω (m)	$10 - 50$	$10^{-4} - 10^{-3}$
$\Delta\xi_{1,2}$ (m)	$0 - 0.5$	$10^{-5} - 10^{-4}$

The initial approximation $\boldsymbol{\theta}_0$ is set from nominal machine parameters and approximate section orientation; $\mathbf{t}_0$ is the centroid of D. The step size α is determined by backtracking line search (Armijo condition, $c = 10^{-4}$, reduction factor 0.5).

Algorithm 1 Gradient descent contour fitting

Input: D, $\boldsymbol{\theta}_0$, $\mathbf{t}_0$, $\varepsilon_{\text{rel}} = 10^{-4}$, $\varepsilon_{\text{err}} = 10^{-6}$, $\varepsilon_{\text{grad}} = 10^{-4}$, $k_{\max} = 500$
$\boldsymbol{\theta} \leftarrow \boldsymbol{\theta}_0$; $\mathbf{t} \leftarrow \mathbf{t}_0$; $E_{\text{prev}} \leftarrow \mathcal{E}(D, \boldsymbol{\theta}, \mathbf{t})$
for $k = 1$ **to** $k_{\max}$ **do**
  $(\nabla_{\boldsymbol{\theta}}, \nabla_{\mathbf{t}}) \leftarrow \nabla\mathcal{E}(D, \boldsymbol{\theta}, \mathbf{t}, \varepsilon_{\text{rel}})$
  $\alpha \leftarrow \alpha_0$
  while $\mathcal{E}(D,\, \boldsymbol{\theta} - \alpha\nabla_{\boldsymbol{\theta}},\, \mathbf{t} - \alpha\nabla_{\mathbf{t}}) > E_{\text{prev}} - c\,\alpha\,\|\nabla E\|^2$ **do**
    $\alpha \leftarrow 0.5\,\alpha$
  end while
  $\boldsymbol{\theta}_{\text{new}} \leftarrow \boldsymbol{\theta} - \alpha\,\nabla_{\boldsymbol{\theta}}$; $\mathbf{t}_{\text{new}} \leftarrow \mathbf{t} - \alpha\,\nabla_{\mathbf{t}}$
  $E_{\text{new}} \leftarrow \mathcal{E}(D, \boldsymbol{\theta}_{\text{new}}, \mathbf{t}_{\text{new}})$
  if $|E_{\text{new}} - E_{\text{prev}}|/|E_{\text{prev}}| < \varepsilon_{\text{err}}$ **or** $\|\nabla E\| < \varepsilon_{\text{grad}}$ **then**
    break
  end if
  $\boldsymbol{\theta} \leftarrow \boldsymbol{\theta}_{\text{new}}$; $\mathbf{t} \leftarrow \mathbf{t}_{\text{new}}$; $E_{\text{prev}} \leftarrow E_{\text{new}}$
end for
Output: $\boldsymbol{\theta}^*$, $\mathbf{t}^*$

After convergence, the 3D position is recovered: $S^* = O + E[S_0^* + \mathbf{t}^*]$, where $S_0^* = \{s_0(u_k; \theta^*)\}_{k=1}^{K}$.

6 Experimental Accuracy Assessment

The accuracy of NP-body parameter recovery is decisive for the applicability of the model. However, direct verification is difficult: trajectory parameters are not monitored during regular surveying, and cross-section contours are constructed schematically from a few width measurements.

Underground laser scanning technology provides a solution. Modern scanners offer high coordinate accuracy and are mobile enough for regular surveying. Mesh surfaces from laser data (Fig. 7a) are not suitable as full 3D models due to holes at blind spots and large data volumes, but can be effectively used for constructing vertical cross-sections. The mine surveyor interactively selects the best-quality section. In the absence of precise trajectory data, the RMS deviation between the loft surface and the scan point cloud (Fig. 7b) is the adequate accuracy metric.

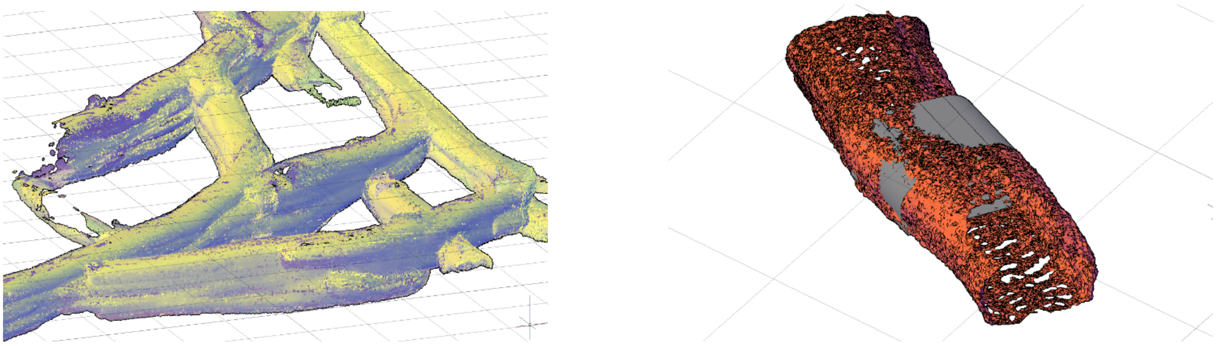

(a) Mesh surface from laser scanning data

(b) Loft representation vs. scan point cloud

Figure 7: Underground laser scanning data and loft representation comparison.

6.1 Experimental Setup

Data from underground laser scanning of production openings at a mining horizon excavated by a Ural-type mining machine ($R = 1.76$, $D = 5.09$, $H = 4.24$, $d = 2.418$, $h = 2.46$) were used. Scan point clouds were constructed using a mobile laser scanning platform (MLSP) with STeAM v2.4 post-processing software. Six datasets were used, averaging 1.5 M points each.

For each point cloud, the highest-quality section was selected and processed with the Scale-Space Surface Reconstruction algorithm (CGAL). The series of vertical cross-sections (Fig. 8) were constructed for the loft representation. The number of NP-bodies was assumed known *a priori*.

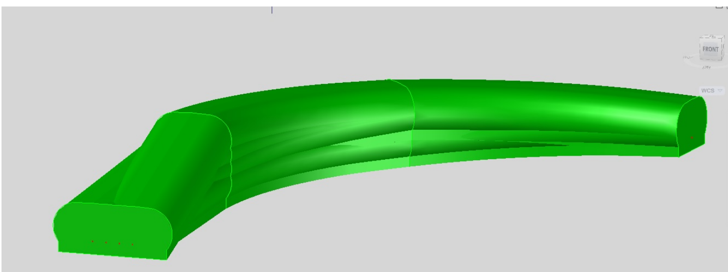

Figure 8: Results of loft-excavation reconstruction.

6.2 Results

For each cross-section and NP-body, the contour fitting algorithm recovered $\theta^*, h^*, \omega^*, \Delta\xi_1^*, \Delta\xi_2^*$. The following were recorded: mean contour deviation from D, number of iterations, and section type (UC — undercut, IS — intersection, IN — inclined). The mean surface deviation from the point cloud was also estimated.

Table 2: Experimental results. UC — undercut, IS — intersection, IN — inclined.

Code	Points	Type 1/2	Iter. 1/2	σ_{sect} 1/2 (m)	σ_{surf} (m)
1290	1.5 M	UC+IN / UC+IS+IN	16 / 31	0.043 / 0.051	0.067
4332	0.8 M	IN / IN	21 / 15	0.031 / 0.029	0.042
4333	1.2 M	IS+IN / IS+IN	30 / 32	0.041 / 0.045	0.056
4334	1.7 M	UC+IS / UC+IS+IN	23 / 14	0.044 / 0.034	0.053
4338	1.8 M	IS+IN / UC+IS+IN	24 / 17	0.047 / 0.035	0.072
4339	0.7 M	IN / IN	22 / 31	0.037 / 0.044	0.058

Contour recovery accuracy is within 0.05 m; surface deviation is 0.07 m. The scanning accuracy is the decisive factor. Surface accuracy is additionally affected by excavation length, trajectory parameter recovery accuracy, and surface noise (power cables, lighting). The experiments confirmed the feasibility of the approach. The small iteration count (14–32) guarantees high construction speed. The accuracy is sufficient for most digital twin tasks: equipment placement, ventilation calculation, transport route planning.

For the experimental parameters (scanning accuracy, noise level, profile parameters, average excavation length 10 m), the volume calculation error is approximately 5%. A potential twofold improvement in scanning accuracy by reducing the excavation length to 5 m is expected to bring the error to approximately 2%.

7 Conclusion

This study addresses the problem of constructing a dynamic 3D model of underground mining space — a core component of digital twins of mining enterprises. The principal challenge lies in balancing geometric accuracy and computational efficiency.

1. Hybrid sweep-loft representation. A specialized geometric representation combining the accuracy of sweep with the non-intersection property of loft has been proposed. Each excavation is decomposed into loft bodies corresponding to individual machine passes, requiring only boundary cross-sections as input.

2. Efficient cross-section algorithm. An analytical algorithm for constructing vertical cross-sections of NP-bodies without explicit 3D surface computation has been developed, exploiting the circular projection property of helical sweep surfaces. Computational complexity is linear in the number of approximation points.

3. Contour fitting algorithm. An inverse problem has been formulated and solved using gradient descent with backtracking line search. Multiple NP-bodies compete for scan points via dynamic nearest-contour assignment.

4. Experimental validation. Validation with underground laser scanning data from a potash deposit demonstrated contour accuracy of 0.05 m, surface deviation of 0.07 m, and convergence in 14–32 iterations.

Limitations

Volume calculation error is ∼5% for 10 m excavations (insufficient for volumetric accounting). The approach depends on scanning quality, requires *a priori* knowledge of the NP-body count, and is currently tailored to Ural-type machines. A larger-scale evaluation is needed.

Future Work

Automatic NP-body count determination; integration into a full digital twin pipeline; computational performance evaluation for complete horizons; extension to other machine types; investigation of alternative optimizers (Levenberg-Marquardt, CMA-ES).

Conflict of Interest

The authors declare no conflict of interest.

References

[1] Cacciuttolo, C. & Atencio, E. Development of an Advanced Multi-Layer Digital Twin Conceptual Framework for Underground Mining. *Sensors*, 2025, vol. 25, no. 21, art. 6650. DOI: 10.3390/s25216650.

[2] Dolgikh, A.S., Senyuk, V.V. & Konovalov, O.L. Creation of a geomechanical support system for underground mining at the Starobin deposit [in Russian]. *Gornyi Zhurnal (Mining Journal)*, 2018, no. 8, pp. 23–28.

[3] Zhang, Y.J. *Geometric Modeling and Mesh Generation from Scanned Images*. Boca Raton: CRC Press, 2018, 364 p. DOI: 10.1201/9781315114170.

[4] Liang, S., Bao, A., Shen, E. & Wang, J. A survey of Boolean operations in 3D geometric modeling. *Computer-Aided Design*, 2026, vol. 197, art. 104081. DOI: 10.1016/j.cad.2026.104081.

[5] Li, Z., Wang, J., Zhu, F. et al. Analysis of point cloud data of tunnel cross-section using cubic B-spline curve. *IOP Conf. Ser.: Earth Environ. Sci.*, 2021, vol. 643, no. 1, art. 012064. DOI: 10.1088/1755-1315/643/1/012064.

[6] Zhao, M., Jia, X., Fan, L., Liang, Y. & Yan, D.-M. Robust Ellipse Fitting Using Hierarchical Gaussian Mixture Models. *IEEE Trans. Image Process.*, 2021, vol. 30, pp. 4443–4456. DOI: 10.1109/TIP.2021.3066855.

[7] Dogrusadik, A. Swept volume cross-section of a general form cutter during 3-axis helical milling. *Int. J. Interact. Des. Manuf.*, 2026. DOI: 10.1007/s12008-026-02559-9.

[8] Abdel-Malek, K. & Yeh, H.J. Formulation of the equations of swept volumes in joint space. *Computer-Aided Design*, 1997, vol. 29, no. 9, pp. 633–646. DOI: 10.1016/S0010-4485(97)00009-8.

[9] Konovalov, O.L. Information modeling of mining enterprise functioning processes [in Russian]. *Vestnik Brest State Technical University. Series: Physics, Mathematics, Informatics*, 2020, no. 5, pp. 9–13.

[10] Yang, Y., Sun, Y. & Wang, Y. Exploring 3D Roadway Modeling Techniques Using CAD and Unity3D. *Processes*, 2025, vol. 13, no. 8, art. 2399. DOI: 10.3390/pr13082399.

[11] Zhang, H., Mao, S. & Li, M. A Coal Mine Excavation Tunnels Modeling Method Based on Point Clouds. *Applied Sciences*, 2024, vol. 14, no. 20, art. 9454. DOI: 10.3390/app14209454.

[12] Cui, Y., Li, J., Li, Y. et al. Multiscale geometric digital twins of mine tunnels that integrate topological evolution and local reconstruction. *Tunnelling and Underground Space Technology*, 2026, vol. 169, art. 107317. DOI: 10.1016/j.tust.2025.107317.